

Bistability of Cavity Magnon Polaritons

Yi-Pu Wang,¹ Guo-Qiang Zhang,¹ Dengke Zhang,^{1,*} Tie-Fu Li,^{2,1,†} C.-M. Hu,³ and J. Q. You^{1,‡}

¹*Quantum Physics and Quantum Information Division, Beijing Computational Science Research Center, Beijing 100193, China*

²*Institute of Microelectronics, Tsinghua National Laboratory of Information Science and Technology, Tsinghua University, Beijing 100084, China*

³*Department of Physics and Astronomy, University of Manitoba, Winnipeg, Manitoba R3T 2N2, Canada*

 (Received 1 August 2017; revised manuscript received 28 November 2017; published 30 January 2018)

We report the first observation of the magnon-polariton bistability in a cavity magnonics system consisting of cavity photons strongly interacting with the magnons in a small yttrium iron garnet (YIG) sphere. The bistable behaviors emerged as sharp frequency switchings of the cavity magnon polaritons (CMPs) and related to the transition between states with large and small numbers of polaritons. In our experiment, we align, respectively, the [100] and [110] crystallographic axes of the YIG sphere parallel to the static magnetic field and find very different bistable behaviors (e.g., clockwise and counter-clockwise hysteresis loops) in these two cases. The experimental results are well fitted and explained as being due to the Kerr nonlinearity with either a positive or negative coefficient. Moreover, when the magnetic field is tuned away from the anticrossing point of CMPs, we observe simultaneous bistability of both magnons and cavity photons by applying a drive field on the lower branch.

DOI: [10.1103/PhysRevLett.120.057202](https://doi.org/10.1103/PhysRevLett.120.057202)

Both quantum information processing [1] and future quantum internet [2] inevitably need efficient quantum information transfers among different physical systems. Hybrid quantum systems may provide hopeful solutions to these problems [3,4]. Recently, cavity magnonics has attracted much interest (see, e.g., [5–12]), which involves cavity photons strongly or ultrastrongly [13] interacting with collective spin excitations in a millimeter-scale yttrium iron garnet (YIG) crystal. This hybrid system gives rise to new quasiparticles called cavity magnon polaritons (CMPs) [14,15]. Benefiting from low damping rates of both magnons and cavity photons, this hybrid system is also expected to become a building block of the future quantum information network. Now, a versatile quantum information processing platform based on the coherent couplings among magnons, cavity microwave photons [5–7], optical photons [16–19], phonons [20], and superconducting qubits [21,22] is being established, with the strong coupling between magnons and cavity photons being the core of the hybrid quantum system.

For the cavity magnonics system, in addition to the hybridization between magnons and cavity photons, the nonlinear effect can also play an important role. Originating from the magnetocrystalline anisotropy in the YIG [23,24], this nonlinearity is related to the Kerr effect of magnons and the nonlinearity-induced frequency shift has been demonstrated in the dispersive regime at cryogenic temperatures [25]. In this Letter, we observe the CMP bistability in a cavity magnonics system. In a wide range of parameters, the frequency of the CMPs is found to jump up or down sharply at the switching points where the CMPs transition

from one state to another. To clearly demonstrate the nonlinear effect, we implement the experiment by aligning the [100] and [110] crystallographic axes of the YIG sphere parallel to the externally applied static magnetic field, respectively. The measured results show very different features in these two cases, such as the blue or red shift of the frequency of the CMPs and the emergence of the clockwise or counterclockwise hysteresis loop related to the CMP bistability. Also, we, theoretically, fit the experimental results well and explain the very different phenomena of the CMPs as being due to the Kerr nonlinearity with either a positive or negative coefficient.

To our knowledge, this Letter is the first convincing observation of the bistability in CMPs. As an important nonlinear phenomenon, bistability is not only of fundamental interest in studying dissipative quantum systems [26,27], but also has potential applications in switches [28,29] and memories [30,31]. Our cavity magnonics system offers a new platform for exploring these applications. Also, the employed Kittle-mode magnons have distinct merits, such as the tunability with magnetic field and the maintenance of good quantum coherence even at room temperature [7,10]. These advantages may bring new possibilities in exploring nonlinear properties of the system. Indeed, we also observe the simultaneous bistability of both magnons and cavity photons at a very off-resonance point by applying a drive field on the lower branch, where the optical bistability is achieved via the magnetic bistability. This observation shows that the CMPs can serve as a bridge or transducer between optical and magnetic bistabilities, which paves a new way for using one effect to induce and control the other.

The experimental setup for our hybrid system is schematically shown in Fig. 1(a). We use a three-dimensional (3D) rectangular cavity made of oxygen-free copper with inner dimensions $44.0 \times 22.0 \times 6.0 \text{ mm}^3$ and have a small YIG sphere of diameter 1 mm glued on an inner wall of the cavity at a magnetic-field antinode of the cavity mode TE_{102} . The cavity has three ports, with ports 1 and 2 as the input and output ports for measuring the transmission spectrum and, also, with a specially designed port (i.e., port 3) in the vicinity of the YIG sphere for conveniently loading a microwave drive field via a loop antenna. Here, we focus on the Kittel mode which is a spatially uniform mode of the ferromagnetic spin waves [32]. To reduce the disturbance from other magnetostatic modes [33,34], the small YIG sphere is placed at the uniform field of the antenna. The whole cavity, with the YIG sphere embedded, is placed in a static magnetic field B_0 created by a high-precision tunable electromagnet at room temperature. This bias magnetic field, the magnetic component of the microwave drive field, and the magnetic field of the TE_{102} mode are nearly perpendicular to one another at the site of the small YIG sphere.

When the frequency of the Kittel-mode magnons is tuned in resonance with the microwave photons of the cavity mode TE_{102} , anticrossing of energy levels occurs owing to the strong coupling between magnons and cavity photons, which gives rise to two branches of CMPs [see Fig. 1(b)]. The magnon-photon coupling strength is found

to be $g_m/2\pi = 41 \text{ MHz}$ from the energy splitting at the resonance (anticrossing) point. The fitted cavity-mode linewidth is $\kappa/2\pi \equiv (\kappa_1 + \kappa_2 + \kappa_3 + \kappa_{\text{int}})/2\pi = 3.8 \text{ MHz}$, where κ_i ($i = 1, 2, 3$) is the decay rate of the cavity due to the i th port and κ_{int} is the intrinsic loss of the cavity. Also, the Kittel-mode linewidth is found to be $\gamma_m/2\pi = 17.5 \text{ MHz}$. It is clear that the system is in the strong-coupling regime because $g_m > \kappa, \gamma_m$.

Here, we demonstrate the nonlinear effect in the cavity magnonics system by driving the YIG sphere with a microwave field via the loop antenna. First, we focus on the case with the magnons in resonance with the cavity photons, where a CMP is the maximal superposition of a magnon and a cavity photon. Also, the YIG sphere is aligned to have its [100] crystallographic axis parallel to the static magnetic field B_0 . In Fig. 2(a), we measure the frequency shift Δ_{LP} of the lower-branch CMPs versus the drive power P_d for different values of the drive-field frequency detuning (see [35] for the measurement method), where the subscript LP denotes the lower-branch polaritons. Here, the angular frequency ω_{LP} of the lower-branch CMPs is tuned to be at the anticrossing point A in Fig. 1(b) and the drive-field frequency detuning $\delta_{\text{LP}} \equiv \omega_{\text{LP}} - \omega_d$ is relative to the lower-branch CMPs, where ω_d is the angular frequency of the drive field. At the resonance point with $\omega_m = \omega_c$ (where ω_m is the frequency of the Kittel-mode magnons and ω_c is the frequency of the cavity mode TE_{102}), a hysteresis loop is clearly seen at $\delta_{\text{LP}} < 0$,

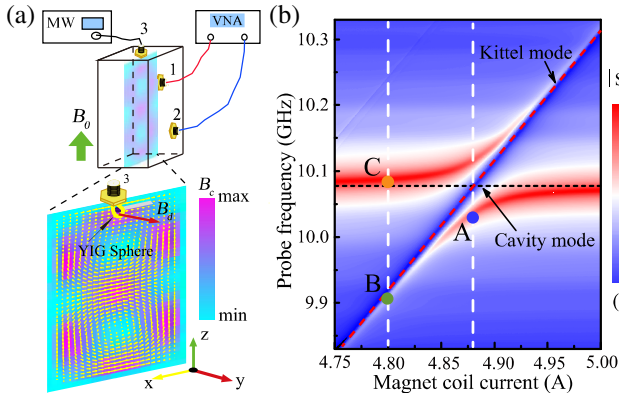


FIG. 1. (a) Schematic diagram of the experimental setup. The 3D cavity, with a small YIG sphere embedded, is placed in the static magnetic field B_0 generated by an electromagnet. Ports 1 and 2 of the cavity, connected to a vector network analyzer (VNA), are used for transmission spectroscopy and port 3, connected to a microwave (MW) source, is for driving the YIG sphere. At the bottom, the magnetic-field distribution of the TE_{102} mode is magnified for clarity. The small YIG sphere is placed beside a circular-loop antenna and located at the magnetic-field antinode of the TE_{102} mode. (b) Transmission spectrum of the CMPs measured versus the magnet coil current (i.e., the static magnetic field) and the frequency of the probe field. Two vertical dashed lines indicate, respectively, the resonance and the very off-resonance points at which we show the CMP bistability.

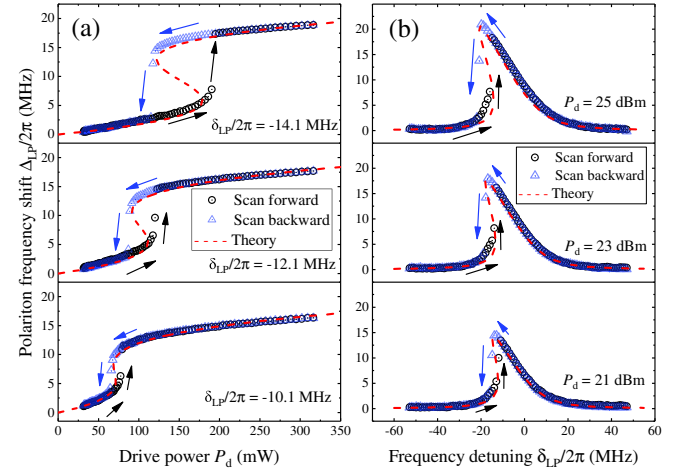


FIG. 2. (a) $\Delta_{\text{LP}}/2\pi$ versus P_d when $\delta_{\text{LP}}/2\pi = -14.1, -12.1,$ and -10.1 MHz . (b) $\Delta_{\text{LP}}/2\pi$ versus $\delta_{\text{LP}}/2\pi$ when $P_d = 25, 23,$ and 21 dBm . The black circle (blue triangle) dots are the forward (backward)-scanning results. The red dashed curves are theoretical results obtained using Eq. (2), with $\gamma_{\text{LP}}/2\pi = (\gamma_m + \kappa)/4\pi = 10.65 \text{ MHz}$. In (a), the characteristic constant $c/(2\pi)^3$ is fitted to be 3.15, 3.55, and 3.82 MHz^3/mW for curves from top to bottom. In (b), $c/(2\pi)^3$ is fitted to be 1.85, 2.52, and 3.22 MHz^3/mW for curves from top to bottom. The [100] crystallographic axis of the YIG sphere is aligned parallel to the static magnetic field B_0 and the magnons are in resonance with the cavity mode TE_{102} .

revealing the emergence of the CMP bistability in the cavity magnonics system. This hysteresis loop is counterclockwise when considering the increasing and decreasing directions of the drive power. Moreover, its area reduces when decreasing the frequency detuning $|\delta_{\text{LP}}|$. In Fig. 2(b), we measure the frequency shift Δ_{LP} of the same lower-branch CMPs versus the frequency detuning δ_{LP} for different values of P_d . When the increasing and decreasing directions of δ_{LP} are considered, a counterclockwise hysteresis loop is also clearly shown, and its area decreases when reducing P_d .

For a small YIG sphere driven by a microwave field with frequency ω_d , when its [100] crystallographic axis is aligned parallel to the static magnetic field, the cavity magnonics system has the Hamiltonian (setting $\hbar = 1$) [25]

$$H = \omega_c a^\dagger a + \omega_m b^\dagger b + Kb^\dagger b b^\dagger b + g_m(a^\dagger b + ab^\dagger) + \Omega_d(b^\dagger e^{-i\omega_d t} + b e^{i\omega_d t}), \quad (1)$$

where $a^\dagger(a)$ is the creation (annihilation) operator of the cavity photons at frequency ω_c , $b^\dagger(b)$ is the creation (annihilation) operator of the Kittel-mode magnons at frequency ω_m , and Ω_d is the drive-field strength. As shown in [25], the Kerr term $Kb^\dagger b b^\dagger b$, with a positive coefficient $K = \mu_0 K_{\text{an}} \gamma^2 / (M^2 V_m)$, is intrinsically due to the magneto-crystalline anisotropy in the YIG material. Here, μ_0 is the magnetic permeability of free space, K_{an} is the first-order anisotropy constant, $\gamma = g\mu_B/\hbar$ is the gyromagnetic ratio (with g being the g factor and μ_B the Bohr magneton), M is the saturation magnetization, and V_m is the volume of the YIG sphere. Note that the Kerr effect is strengthened when reducing V_m .

We consider the case with $|\omega_{\text{LP}} - \omega_d| \ll |\omega_{\text{UP}} - \omega_d|$, where ω_{UP} is angular frequency of the upper-branch CMPs (which are denoted by the subscript UP). In such a case, the drive field applied to the YIG sphere generates polaritons in the lower branch much more than the polaritons in the upper branch. Using a quantum Langevin approach, we obtain a cubic equation for the CMP frequency shift Δ_{LP} [35]

$$\left[(\Delta_{\text{LP}} + \delta_{\text{LP}})^2 + \left(\frac{\gamma_{\text{LP}}}{2} \right)^2 \right] \Delta_{\text{LP}} - cP_d = 0, \quad (2)$$

where γ_{LP} is the damping rate of the lower-branch CMP and c is a coefficient characterizing the coupling strength between the drive field and the lower-branch CMPs. This cubic equation provides a steady-state solution for the frequency shift of the lower-branch CMPs as a function of both the drive-field frequency detuning δ_{LP} and the drive power P_d . Under appropriate conditions, it has three solutions, two of them stable and the additional one unstable. This corresponds to the bistability of the system. In Fig. 2, we also show the theoretical results (dashed curves) obtained using Eq. (2), which fit the experimental

results very well. This verifies the experimental observation of the CMP bistability in our cavity magnonics system. The two stable solutions of Δ_{LP} in Eq. (2) correspond to two states of the system with large and small numbers of polaritons in the lower branch [35]. Thus, in Fig. 2, each sharp switching of the frequency shift Δ_{LP} is related to the transition between these two states.

In the resonance case with $\omega_m = \omega_c$, we further implement experiment by aligning the [110] crystallographic axis of the YIG sphere parallel to the static magnetic field B_0 . In Fig. 3(a), we measure the frequency shift Δ_{LP} of the lower-branch CMPs versus the drive power P_d for different values of the drive-field frequency detuning δ_{LP} relative to the lower-branch CMPs. In sharp contrast to Fig. 2(a), bistability of the lower-branch CMPs is now observed at $\delta_{\text{LP}} > 0$. The area of the hysteresis loop also decreases when reducing δ_{LP} , but the hysteresis loop becomes clockwise. Also, we present, in Fig. 3(b), the frequency shift Δ_{LP} versus the frequency detuning δ_{LP} for different values of P_d . The hysteresis loop is also counterclockwise, similar to that in Fig. 2(b).

As shown in [35], when the YIG sphere is aligned with its [110] crystallographic axis parallel to the static magnetic field B_0 , the Hamiltonian of the cavity magnonics system takes the same form as in Eq. (1), but the coefficient of the Kerr term becomes negative, $K = -13\mu_0 K_{\text{an}} \gamma^2 / (16M^2 V_m)$. The corresponding theoretical results (dashed curves) obtained using Eq. (2) are shown in Fig. 3, which are also in good agreement with the experimental results.

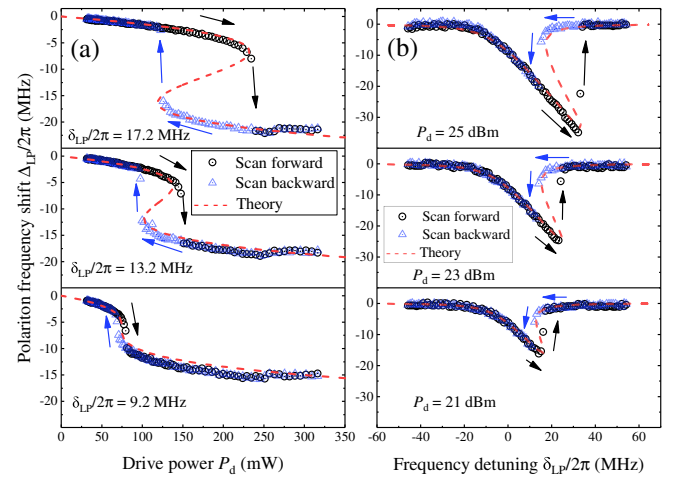


FIG. 3. (a) $\Delta_{\text{LP}}/2\pi$ versus P_d when $\delta_{\text{LP}}/2\pi = 17.2, 13.2,$ and 9.2 MHz. (b) $\Delta_{\text{LP}}/2\pi$ versus $\delta_{\text{LP}}/2\pi$ when $P_d = 25, 23,$ and 21 dBm. The black circle (blue triangle) dots are the forward (backward)-scanning results. The red dashed curves are theoretical results obtained using Eq. (2), with $\gamma_{\text{LP}}/2\pi = 10.65$ MHz. In (a), $c/(2\pi)^3$ is fitted to be $-4, -3.5,$ and -3.1 MHz^3/mW for curves from top to bottom. In (b), $c/(2\pi)^3$ is fitted to be $-3.01, -3.46,$ and -3.6 MHz^3/mW for curves from top to bottom. The [110] crystallographic axis of the YIG sphere is aligned parallel to B_0 and the magnons are in resonance with TE_{102} .

Moreover, Figs. 2 and 3 show that the CMPs have blueshift (redshift) in frequency when the [100] ([110]) crystallographic axis of the YIG sphere is aligned along the direction of the static magnetic field. These are due to the positive and negative Kerr coefficients K_s in the two different cases [35].

Finally, we demonstrate the Kerr effect of magnons at an off-resonance point much away from $\omega_m = \omega_c$, where the magnet coil current is 4.8 A [see the left dashed line in Fig. 1(b)]. At this point, the frequency of the lower-branch CMPs is about 9.91 GHz and the frequency of the upper-branch CMPs is about 10.08 GHz, as indicated by points *B* and *C* in Fig. 1(b), respectively. Also, the [100] crystallographic axis of the YIG sphere is aligned parallel to the static magnetic field B_0 . In Fig. 4(a), we present the frequency shift Δ_{LP} of the lower-branch CMPs versus the drive power P_d for different values of the drive-field frequency detuning δ_{LP} relative to the lower-branch CMPs. Moreover, the frequency shift Δ_{LP} versus the frequency detuning δ_{LP} is shown in Fig. 4(b) for different values of P_d . As in Fig. 2, we also see counterclockwise hysteresis loops. Because the magnon is a dominating component of the lower-branch CMP at this very off-resonance point, nearly all of the bistability of magnons is actually observed here, directly owing to the magnon Kerr effect in the YIG sphere. The theoretical results (dashed curves) obtained using Eq. (2) also agree well with the experimental results.

Under the same conditions as in Figs. 4(a) and 4(b), we further show the frequency shift Δ_{UP} of the upper-branch CMPs versus the drive power P_d [Fig. 4(c)], as well as the frequency shift Δ_{UP} of the upper-branch CMPs versus the drive-field frequency detuning δ_{LP} relative to the lower-branch CMPs [Fig. 4(d)]. Here, as in Figs. 4(a) and 4(b), the drive field is still applied on the lower branch. Now the cavity photon is a dominating component of the upper-branch CMP at this very off-resonance point, so it is nearly all the bistability of cavity photons that is observed in Figs. 4(c) and 4(d). As one knows, both optical [40,41] and magnetic [42] bistabilities are interesting phenomena of nonlinear systems. Here, we observe the simultaneous bistability of both magnons and cavity photons at a very off-resonance point by applying the drive field only on the lower branch, where the optical bistability is achieved via the magnetic bistability. Also, the experimental results in Figs. 4(c) and 4(d) fit well with the theoretical results (dashed curves), where the fitted ratio $\xi \equiv \Delta_{UP}/\Delta_{LP}$ is close to the theoretical value 0.065 [35]. In addition, some small dips are observed in, e.g., Figs. 4(c) and 4(d). By fitting with these dips, we attribute them to other polaritons stemming from the coupling between cavity photons and a magnetostatic mode with the negative Kerr coefficient [35].

In conclusion, we have demonstrated the bistable behaviors of the CMPs using a hybrid system consisting of microwave cavity photons strongly interacting with the magnons in a YIG sphere. We find that the switching points

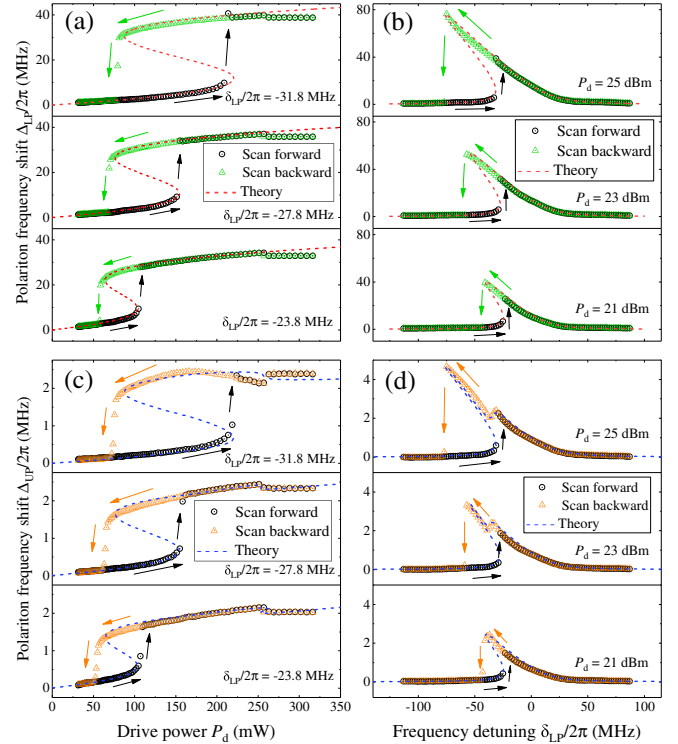


FIG. 4. (a) $\Delta_{LP}/2\pi$ versus P_d when $\delta_{LP}/2\pi = -31.8$, -27.8 , and -23.8 MHz. (b) $\Delta_{LP}/2\pi$ versus $\delta_{LP}/2\pi$ when $P_d = 25$, 23, and 21 dBm. The black circle (green triangle) dots are the forward (backward)-scanning results. The red dashed curves are theoretical results obtained using Eq. (2), with $\gamma_{LP}/2\pi = 16.8$ MHz. In (a), $c/(2\pi)^3$ is fitted to be 25.2, 25.0, and 25.3 MHz³/mW for curves from top to bottom. In (b), $c/(2\pi)^3$ is fitted to be 17.0, 19.0, and 22.7 MHz³/mW for curves from top to bottom. (c) and (d) $\Delta_{UP}/2\pi$ measured under the same conditions as in (a) and (b), respectively. The black circle (orange triangle) dots are the forward (backward)-scanning results. The blue dashed curves (except for the parts around small dips) are also obtained using Eq. (2), with the fitted ratio $\xi \equiv \Delta_{UP}/\Delta_{LP}$ for curves from top to bottom being 0.060, 0.062, and 0.061 in (c) and 0.062, 0.063, and 0.061 in (d). The [100] crystallographic axis of the YIG sphere is aligned parallel to B_0 and the magnons are far off resonance with TE₁₀₂. In addition, the small dips in, e.g., (c) and (d) can be fitted by introducing a magnetostatic mode with the negative Kerr coefficient [35].

where the CMPs transition from one state to another depend on the drive power and the drive-field frequency detuning. When implementing the experiment, we align, respectively, the [100] and [110] crystallographic axes of the YIG sphere parallel to the static magnetic field and find very different bistable behaviors in these two cases. We, theoretically, fit the experimental results well and put these different bistable behaviors down to the Kerr nonlinearity with either a positive or negative coefficient.

The cavity magnonics system possesses the merits of tunability and compatibility with other quantum systems, in which the magnons can be tuned by an external magnetic field and the magnon-photon coupling can be tuned by

moving the YIG sphere inside the cavity. With regard to the bistability of the CMPs, the area of the hysteresis loop can be easily controlled by a lower drive power and a tunable drive-field frequency. This may bring potential applications in realizing low-energy switching devices. Also, we observe simultaneous bistability of both magnons and cavity photons by tuning the magnetic field. It paves a new path for controlling the conversion between magnetic and optical bistabilities. Moreover, our study provides possible routes for exploring other nonlinear effects of the system such as the creation of a frequency comb for frequency conversion [43] and the chaos of CMPs. With the available CMP bistability, the cavity magnonics system can also provide a new platform for understanding the dissipative phase transition and the related critical phenomena [26,44,45]. These open up different directions for future studies.

This work was supported by the National Key Research and Development Program of China (Grant No. 2016YFA0301200), the NSFC (Grant No. 11774022), the MOST 973 Program of China (Grant No. 2014CB848700), the NSAF (Grants No. U1330201 and No. U1530401), and the Science Challenge Project (Grant No. TZ2017003). C. M. H. was supported by the NSFC (Grant No. 11429401).

Y.-P. W and G.-Q. Z contributed equally to this work.

*Present address: Department of Engineering, University of Cambridge, Cambridge CB3 0FA, United Kingdom.

[†]litf@tsinghua.edu.cn

[‡]jqyou@csrc.ac.cn

- [1] M. Wallquist, K. Hammerer, P. Rabl, M. Lukin, and P. Zoller, Hybrid quantum devices and quantum engineering, *Phys. Scr.* **T137**, 014001 (2009).
- [2] H. J. Kimble, The quantum internet, *Nature (London)* **453**, 1023 (2008).
- [3] Z.-L. Xiang, S. Ashhab, J. Q. You, and F. Nori, Hybrid quantum circuits: Superconducting circuits interacting with other quantum systems, *Rev. Mod. Phys.* **85**, 623 (2013).
- [4] G. Kurizki, P. Bertet, Y. Kubo, K. Mølmer, D. Petrosyan, P. Rabl, and J. Schmiedmayer, Quantum technologies with hybrid systems, *Proc. Natl. Acad. Sci. U.S.A.* **112**, 3866 (2015).
- [5] H. Huebl, C. W. Zollitsch, J. Lotze, F. Hocke, M. Greifenstein, A. Marx, R. Gross, and S. T. B. Goennenwein, High Cooperativity in Coupled Microwave Resonator Ferrimagnetic Insulator Hybrids, *Phys. Rev. Lett.* **111**, 127003 (2013).
- [6] Y. Tabuchi, S. Ishino, T. Ishikawa, R. Yamazaki, K. Usami, and Y. Nakamura, Hybridizing Ferromagnetic Magnons and Microwave Photons in the Quantum Limit, *Phys. Rev. Lett.* **113**, 083603 (2014).
- [7] X. Zhang, C.-L. Zou, L. Jiang, and H. X. Tang, Strongly Coupled Magnons and Cavity Microwave Photons, *Phys. Rev. Lett.* **113**, 156401 (2014).
- [8] M. Goryachev, W. G. Farr, D. L. Creedon, Y. Fan, M. Kostylev, and M. E. Tobar, High-Cooperativity Cavity QED with Magnons at Microwave Frequencies, *Phys. Rev. Applied* **2**, 054002 (2014).
- [9] L. Bai, M. Harder, Y. P. Chen, X. Fan, J. Q. Xiao, and C.-M. Hu, Spin Pumping in Electro-dynamically Coupled Magnon-Photon Systems, *Phys. Rev. Lett.* **114**, 227201 (2015).
- [10] D. Zhang, X.-M. Wang, T.-F. Li, X.-Q. Luo, W. Wu, F. Nori, and J. Q. You, Cavity quantum electrodynamics with ferromagnetic magnons in a small yttrium-iron-garnet sphere, *npj Quantum Inf.* **1**, 15014 (2015).
- [11] Ó. O. Soykal and M. E. Flatté, Strong Field Interactions between a Nanomagnet and a Photonic Cavity, *Phys. Rev. Lett.* **104**, 077202 (2010).
- [12] B. Z. Rameshti, Y. Cao, and G. E. W. Bauer, Magnetic spheres in microwave cavities, *Phys. Rev. B* **91**, 214430 (2015).
- [13] J. Bourhill, N. Kostylev, M. Goryachev, D. L. Creedon, and M. E. Tobar, Ultrahigh cooperativity interactions between magnons and resonant photons in a YIG sphere, *Phys. Rev. B* **93**, 144420 (2016).
- [14] Y. Cao, P. Yan, H. Huebl, S. T. B. Goennenwein, and G. E. W. Bauer, Exchange magnon-polaritons in microwave cavities, *Phys. Rev. B* **91**, 094423 (2015).
- [15] B. M. Yao, Y. S. Gui, Y. Xiao, H. Guo, X. S. Chen, W. Lu, C. L. Chien, and C.-M. Hu, Theory and experiment on cavity magnon-polariton in the one-dimensional configuration, *Phys. Rev. B* **92**, 184407 (2015).
- [16] A. Osada, R. Hisatomi, A. Noguchi, Y. Tabuchi, R. Yamazaki, K. Usami, M. Sadgrove, R. Yalla, M. Nomura, and Y. Nakamura, Cavity Optomagnonics with Spin-Orbit Coupled Photons, *Phys. Rev. Lett.* **116**, 223601 (2016).
- [17] X. Zhang, N. Zhu, C.-L. Zou, and H. X. Tang, Optomagnonic Whispering Gallery Microresonators, *Phys. Rev. Lett.* **117**, 123605 (2016).
- [18] J. A. Haigh, A. Nunnenkamp, A. J. Ramsay, and A. J. Ferguson, Triple-Resonant Brillouin Light Scattering in Magneto-Optical Cavities, *Phys. Rev. Lett.* **117**, 133602 (2016).
- [19] C. Braggio, G. Carugno, M. Guarise, A. Ortolan, and G. Ruoso, Optical Manipulation of a Magnon-Photon Hybrid System, *Phys. Rev. Lett.* **118**, 107205 (2017).
- [20] X. Zhang, C.-L. Zou, L. Jiang, and H. X. Tang, Cavity magnomechanics, *Sci. Adv.* **2**, e1501286 (2016).
- [21] Y. Tabuchi, S. Ishino, A. Noguchi, T. Ishikawa, R. Yamazaki, K. Usami, and Y. Nakamura, Coherent coupling between a ferromagnetic magnon and a superconducting qubit, *Science* **349**, 405 (2015).
- [22] D. Lachance-Quirion, Y. Tabuchi, S. Ishino, A. Noguchi, T. Ishikawa, R. Yamazaki, and Y. Nakamura, Resolving quanta of collective spin excitations in a millimeter-sized ferromagnet, *Sci. Adv.* **3**, e1603150 (2017).
- [23] D. D. Stancil and A. Prabhakar, *Spin Waves* (Springer, Berlin, 2009).
- [24] A. G. Gurevich and G. A. Melkov, *Magnetization Oscillations and Waves* (CRC, Boca Raton, FL, 1996).
- [25] Y. P. Wang, G. Q. Zhang, D. Zhang, X. Q. Luo, W. Xiong, S. P. Wang, T. F. Li, C.-M. Hu, and J. Q. You, Magnon Kerr effect in a strongly coupled cavity-magnon system, *Phys. Rev. B* **94**, 224410 (2016).

- [26] S. R. K. Rodriguez, W. Casteels, F. Storme, N. Carlon Zambon, I. Sagnes, L. Le Gratiet, E. Galopin, A. Lemaître, A. Amo, C. Ciuti, and J. Bloch, Probing a Dissipative Phase Transition via Dynamical Optical Hysteresis, *Phys. Rev. Lett.* **118**, 247402 (2017).
- [27] F. Letscher, O. Thomas, T. Niederprüm, M. Fleischhauer, and H. Ott, Bistability versus Metastability in Driven Dissipative Rydberg Gases, *Phys. Rev. X* **7**, 021020 (2017).
- [28] T. K. Paraíso, M. Wouters, Y. Leéger, F. Morier-Genoud, and B. Deveaud-Plédran, Multistability of a coherent spin ensemble in a semiconductor microcavity, *Nat. Mater.* **9**, 655 (2010).
- [29] O. R. Bilal, A. Foehr, and C. Daraio, Bistable metamaterial for switching and cascading elastic vibrations, *Proc. Natl. Acad. Sci. U.S.A.* **114**, 4603 (2017).
- [30] E. Kuramochi, K. Nozaki, A. Shinya, K. Takeda, T. Sato, S. Matsuo, H. Taniyama, H. Sumikura, and M. Notomi, Large-scale integration of wavelength-addressable all-optical memories on a photonic crystal chip, *Nat. Photonics* **8**, 474 (2014).
- [31] V. Kubytzkyi, S.-A. Biehs, and P. Ben-Abdallah, Radiative Bistability and Thermal Memory, *Phys. Rev. Lett.* **113**, 074301 (2014).
- [32] C. Kittel, On the theory of ferromagnetic resonance absorption, *Phys. Rev.* **73**, 155 (1948).
- [33] L. R. Walker, Resonant modes of ferromagnetic spheroids, *J. Appl. Phys.* **29**, 318 (1958).
- [34] P. C. Fletcher and R. O. Bell, Ferrimagnetic resonance modes in spheres, *J. Appl. Phys.* **30**, 687 (1959).
- [35] See Supplemental Material at <http://link.aps.org/supplemental/10.1103/PhysRevLett.120.057202> for the measurement method, Hamiltonian of the cavity magnonics system, steady-state behavior of the cavity magnonics system, and small dips due to other polaritons, which includes Refs. [36–39].
- [36] S. Blundell, *Magnetism in Condensed Matter* (Oxford University Press, Oxford, 2001).
- [37] J. R. Macdonald, Resonant modes of ferromagnetic spheroids, *Proc. Phys. Soc. London Sect. A* **64**, 968 (1951).
- [38] T. Holstein and H. Primakoff, Field dependence of the intrinsic domain magnetization of a ferromagnet, *Phys. Rev.* **58**, 1098 (1940).
- [39] D. F. Walls and G. J. Milburn, *Quantum Optics* (Springer, Berlin, 1994).
- [40] A. Baas, J. Ph. Karr, H. Eleuch, and E. Giacobino, Optical bistability in semiconductor microcavities, *Phys. Rev. A* **69**, 023809 (2004).
- [41] H. Gibbs, *Optical Bistability: Controlling Light with Light* (Academic Press, Orlando, 2012).
- [42] Y. S. Gui, A. Wirthmann, N. Mecking, and C.-M. Hu, Direct measurement of nonlinear ferromagnetic damping via the intrinsic foldover effect, *Phys. Rev. B* **80**, 060402 (2009).
- [43] D. L. Creedon, K. Benmessai, and M. E. Tobar, Frequency Conversion in a High Q-Factor Sapphire Whispering Gallery Mode Resonator due to Paramagnetic Nonlinearity, *Phys. Rev. Lett.* **109**, 143902 (2012); D. L. Creedon, K. Benmessai, W. P. Bowen, and M. E. Tobar, Four-Wave Mixing from Fe^{3+} Spins in Sapphire, *Phys. Rev. Lett.* **108**, 093902 (2012).
- [44] E. M. Kessler, G. Giedke, A. Imamoglu, S. F. Yelin, M. D. Lukin, and J. I. Cirac, Dissipative phase transition in a central spin system, *Phys. Rev. A* **86**, 012116 (2012).
- [45] C. Carr, R. Ritter, C. G. Wade, C. S. Adams, and K. J. Weatherill, Nonequilibrium Phase Transition in a Dilute Rydberg Ensemble, *Phys. Rev. Lett.* **111**, 113901 (2013).